Nitrous oxide (N₂O) processing for silicon oxynitride gate dielectrics

by K. A. Ellis R. A. Buhrman

The gas-phase chemistry of silicon oxynitridation in N₂O has been investigated. From an evaluation of available kinetic data, we have developed a model for the thermal decomposition of gaseous N₂O. To quantify heat transfer between the N₂O gas and the wall of the furnace, we introduce the concept of referencing to an N₂ gas-temperature profile, measured in an oxidation furnace. Using this model, we can account for the increase with flow rate and temperature of the NO concentration in the N₂O decomposition product, and the self-heating during decomposition, for furnace processing. This change in gaseous NO concentration translates to a higher nitrogen content and lower growth rate for the silicon oxynitride. For rapid thermal and other short-gas-residencetime systems, we show that atomic oxygen is present at the Si wafer, and that this removes previously incorporated nitrogen.

Introduction

The gate oxide is a fundamental component of an MOS (metal-oxide-silicon) structure upon which MOSFETs

(MOS field-effect transistors) are based. The standard by which all other gate oxides are measured is pure SiO₂. This material, and any other potential gate dielectrics, must withstand high electric fields, contain few electrical defects, and be robust with respect to damage during operation of the device.

Recently, the 1997 National Technology Roadmap for Semiconductors [1] identified several potential deficiencies for SiO_2 : high leakage currents for films below 2 nm, due to direct tunneling between the gate and substrate; out-diffusion from the heavily boron-doped gate in p-MOSFETs, and penetration of this boron into the channel of the device; and charge-induced damage and breakdown during device operation.

Due to its ability to ameliorate the last two of these deficiencies, lightly nitrided silicon dioxide has been of relatively longstanding interest as an alternative to SiO₂. These dielectrics, referred to as oxynitrides, can generally be regarded as a slight modification of pure SiO₂, and contain only a few percent nitrogen. Since SiO₂ is typically grown in pure O₂ at high temperature, in either a furnace or rapid thermal processor (RTP), growing an oxynitride appears to be as simple as substituting NH₃, N₂O, or NO gas for O₂ and altering the growth recipe. However, for the second of these gases, N₂O, the gas-phase chemistry of oxynitride processing is quite complicated, as this paper reveals.

[®]Copyright 1999 by International Business Machines Corporation. Copying in printed form for private use is permitted without payment of royalty provided that (1) each reproduction is done without alteration and (2) the *Journal* reference and IBM copyright notice are included on the first page. The title and abstract, but no other portions, of this paper may be copied or distributed royalty free without further permission by computer-based and other information-service systems. Permission to *republish* any other portion of this paper must be obtained from the Editor.

0018-8646/99/\$5.00 © 1999 IBM

The first of these three gases used to produce thermal oxynitrides, NH_3 , is a child of the 1980s [2], although interest in it has reappeared owing to the need for higher nitrogen concentrations in the prevention of boron penetration. In the 1990s, NH_3 was largely supplanted by N_2O and NO for processing gate dielectrics [3–7]. The advantages of N_2O and NO are improved reliability [3, 8–12], suppression of H transport [13], and reduction of boron penetration from doped polycrystalline-Si gates [14–17] by the occlusion of diffusion pathways [18, 19]. Counterbalancing these advantages are the degradation of channel mobility under certain conditions [8, 10, 12], and increased thermal budget.

One additional disadvantage, specific to N₂O processing, is complexity. Both the growth rate and the nitrogen content are affected by temperature [20-24] and flow rate [21, 24-27]. These effects are caused by differences in the NO/O, ratio at the Si wafer surface, which is a function of the precise temperature history of the gas: At low flow rates, the N₂O decomposes at least partially in the cooler regions of the inlet; at high flow rates, decomposition heats the inlet, resulting in a higher NO/O2 ratio and thus more nitrogen incorporated into the oxynitride gate dielectric [26]. In addition, systems with a sufficiently short gas residence time at high temperature can remove previously incorporated nitrogen from the oxynitride [28–30] due to the presence of atomic oxygen [29]. The complexity of this process is a disadvantage which fortunately can be mitigated, and even rendered useful, with sufficient understanding.

Some early steps toward understanding this system have been taken recently by Hartig and Tobin, who attempted to model the decomposition of N_2O [31]. Although their model introduced the interesting possibility that H_2O contamination can be disastrous for NO yield, they were not able to compare their results to experimental data. There is also some question regarding the best selection of reaction rate constants and their error limits, given the variability found in the literature on N_2O decomposition reactions.

In this paper, we take further steps and present a new method for modeling N₂O decomposition. We first summarize the decomposition chemistry, and undertake a review of the relevant published rate constants, based primarily on the handbook by Baulch et al. [32, 33]. However, for certain reactions at typical oxynitridation temperatures, the available rate data are incomplete. In these cases we estimate rates and error limits, and discuss their effect on gas-phase modeling. We then introduce a new technique for modeling gas temperatures, in which furnace temperature profiles measured in N₂ are used as the basis for calculating N₂O gas temperatures in the same furnace. This technique offers a significant improvement over the method employed by Hartig and Tobin [31]. With

this model, we can account for the measured dependence of gas temperature and NO concentration on N_2O flow rate and furnace wall temperature, as well as the salient features of N_2O oxynitridation of Si in RTP and high-flow-rate furnaces.

Decomposition chemistry

Understanding gas-phase chemistry is key to understanding N_2O oxynitridation. Specifically, there are two important factors: where the gas decomposes in relation to the wafer, and its precise temperature history during decomposition. These two factors determine the composition of the growth ambient, and therefore the nitrogen content and growth rate of the oxynitride.

The first step in the decomposition of N_2O is unimolecular dissociation into N_2 and O (atomic oxygen):

$$N_2O + M \rightarrow N_2 + O + M. \tag{R1}$$

The atomic oxygen liberated in (R1) is rapidly consumed by one of the following reactions:

$$O + O + M \rightarrow O_2 + M, \tag{R2}$$

$$O + N_2O \rightarrow 2 NO,$$
 (R3)

$$O + N_2O \rightarrow N_2 + O_2, \qquad (R4)$$

$$O + NO + M \rightarrow NO_2 + M_2$$
 (R5)

$$O + NO_2 \rightarrow NO + O_2$$
, (R6)

$$O + wall \rightarrow 1/2 O_2$$
, (R7)

Here M are collision partners which affect the reaction rate. The NO_2 produced in (R5) caused some early confusion [25], but it is now recognized that any NO_2 produced during decomposition rapidly and completely dissociates into NO and O_2 at typical furnace temperatures [26, 31, 34, 35]:

$$2 \text{ NO}_2 \rightarrow 2 \text{ NO} + O_2$$
. (R8)

It is significant that reactions (R5), (R6), and (R8) do not affect the total concentration of NO_x species. Therefore, the only mechanism for NO_x creation is (R3) [32, 33].

The end result of complete N_2O decomposition is a mixture of N_2 , O_2 , and NO. As noted, at high temperature NO_2 is present only as an intermediate species. Once decomposition is complete, this mixture is stable, although at temperatures below 600°C significant conversion from NO to NO_2 may occur. The relative concentrations of the gases in this stable state depend on the precise temperature history during decomposition.

• Reaction rate constants

Some insight into the details of N₂O decomposition can be gained by studying what is known about the various rate constants for reactions (R1–R8). We present a reaction-

by-reaction summary based on the comprehensive reviews by Baulch et al. [32, 33] unless otherwise noted. In some cases, however, the information is incomplete or unreliable. We therefore urge caution in selecting among the various published reaction rates. After motivating our own selection of rate constants, we use these values to construct a model for N_2O decomposition for which we can estimate the error, and which can be compared to our earlier experimental observations [26].

The reaction rate constants of (R1–R8) are given by k_1 through k_8 . For example, at atmospheric pressure, (R1) follows a second-order rate equation, represented by the first term in the total rate equation for N₂O:

$$\frac{d}{dt}[N_2O] = -k_1[N_2O][M] - (k_3 + k_4)[O][N_2O]. \tag{1}$$

Here [x] represents the concentration of gas x in mol/cc. The rate constant k_1 is defined by a set of rate coefficients, within a given temperature range, which are derived from the Arrhenius equation:

$$k = A \exp\left(\frac{-E_{\rm a}}{k_{\rm b}T}\right);\tag{2}$$

 $E_{\rm a}$ is the activation energy in eV, and $k_{\rm b}$ is Boltzmann's constant. A is an exponential pre-factor, the exact units of which, in mol-cm-s, vary depending on the order of the rate equation. Table 1 gives the Arrhenius factors of each reaction, along with notes which are discussed in the text.

Several of the reactions, (R1), (R2), and (R5), include collision-partner efficiencies, indicated by [M]. This indicates a process which can be collision-activated. The efficiency of this method of activation may or may not depend on the species M involved. We are most concerned with $M = N_2O$ early in the decomposition process, shifting toward $M = O_2$, N_2 , NO as the process nears completion.

We begin our survey of the reactions with (R1). At pressures below 10⁻⁴ mol/cc, which includes all atmospheric pressure furnace and RTP processing, it approximately follows the second-order rate equation given in Equation (1) [32, 36]. In our case, $M = N_2O$ is the most important collision-partner efficiency early in the decomposition. Unfortunately, reliable rate data for $M = N_2O$ are sparse, and limited to 900-1050 K. The system shifts toward $M = N_2$, O_2 , NO as decomposition progresses, for which rate data exist only above 1300 K. The rate coefficients for both ranges, as recommended by Baulch et al., are shown in Table 1. The available data therefore present two obstacles for accurate modeling: There is a temperature gap in k_1 coinciding with the region in which we are most interested, 1050-1300 K; and data on collision-partner efficiencies are incomplete.

There have been attempts to determine the relative efficiencies of the various M, but there are no clear

Table 1 Arrhenius factors for the various rate constants k_n , corresponding to reactions (R1–R8). A and E_a are defined in Equation (2). k_1 , k_1' , k_1'' , and k_2 were applied for all values of M, k_3 and k_4 were applied at all temperatures; other reactions were applied only within the quoted temperature range. The error limits are given as either a multiplicative constant or \pm a percentage uncertainty. All data from Baulch et al. [32, 33], except \dagger , which indicates an interpolation between the endpoints of k_1 and k_1' , and \ddagger , which indicates our estimate based on data reviewed by Baulch et al.

Rate constant	A (cm-mol-s)	$\frac{E_{\rm a}}{({ m eV})}$	Error	Note
k_1	5.0×10^{14}	2.50	1.5	1300-2500 K
k_1'	2.7×10^{15}	2.57	1.5	900-1050 K
k_{1}''	1.1×10^{13}	2.07	1.5	1050-1300 K,†
$k_{_2}$	1.9×10^{13}	0.078	±60%	
k_3	1.0×10^{14}	1.21	2	$k_3/k_4 = 1 \pm 0.25$
$k_{_4}$	1.0×10^{14}	1.21	2.5	
$k_{_{5}}$	1.1×10^{15}	-0.081	2.7‡	$M = O_2$
	2.0×10^{15}	-0.081	5‡	$M = N_2 \ddagger$
	3.0×10^{15}	-0.081	5‡	$M = N_2O, NO\ddagger$
$k_{_{6}}$	1.0×10^{13}	0.026	±50%	Extrapolation‡
k_{7}	-	_	_	Negligible
k_8	2.0×10^{12}	1.16	±30%	

trends, and Baulch et al. are unable to make recommendations. Lacking complete data, we have therefore assumed that the efficiencies of the relevant species for (R1) are identical.

As for the temperature gap, we use k_1 to indicate the recommended value from 900–1050 K, and k_1' for 1300–2500 K. Both rate constants were used over their respective temperature ranges. For temperatures between 1050 K and 1300 K, we used the interpolation k_1'' from Table 1. The values for A and E_a for k_1'' were calculated from an interpolation between the endpoints of k_1 and k_1' . These values should only be used over the range 1050–1300 K, and E_a for k_1'' should not be interpreted as the activation energy for (R1), but as a fitting parameter for the interpolation.

Moving to Reaction (R2), we find that it suffers from collision-partner complications similar to those of (R1). The only reliable data in our temperature range are for M = Ar, for which extracted rate constants are quoted in Table 1. Data for $M = \text{N}_2\text{O}$, O_2 , N_2 at high temperature are unreliable, so we have no way to directly determine the rate constant for these gases. Lacking sufficient data, we therefore use the M = Ar data as a best guess and assume that all collision-partner efficiencies are identical.

The spread in the data is quite large, and therefore the error limits on this rate constant are considerable.

Reactions (R3) and (R4) are the principal mechanisms for O deactivation in the early stages of decomposition. (R3) is critical because of its role in generating NO, and it has been the subject of more direct investigations than (R4). Baulch et al. conclude that the ratio k_3/k_4 is unitary within a factor of 1.25, so in propagating the error for the rate constants, we used the error limit for k_3 , and assumed $k_4 = k_3$ to within the factor of 1.25.

Reaction (R5) is the principal mechanism for O deactivation in the later stages of decomposition. Information on the rate of this reaction at high temperature is unfortunately quite unreliable. Baulch et al. recommend a value only for the temperature range of 200-500 K and for $M = O_2$, Ar. Rate information for the chemiluminescence deactivation of NO, associated with (R5) has been measured above 500 K; however, extraction of k_s from chemiluminescent intensities is not possible. Lacking better information, we extend Baulch's recommendation to higher temperatures. At 2000 K, the value for k_5 calculated from Table 1 is known to be off by a factor of 2.7 on the basis of the inverse reaction (k_{5}) and the equilibrium state [32]. We therefore consider 2.7 to be a reasonable estimate for the error limits in our temperature range. Rate data for $M = N_0O$, NO, N_0 are also sparse. On the basis of data reviewed by Baulch et al. (his references 3, 4, 15, 50, 109, 111), we estimate the enhanced efficiency of N₂ to be a factor of 2, and the enhancement of N₂O and NO to be a factor of 3. However, in estimating these efficiencies, we extend the error limits for $M = N_2O$, NO, N_2 to a factor of 5.

A more recent paper concerning Reaction (R5) by Yarwood et al. [37], conducted at low pressure and with M = Ar, agrees with this extrapolation over the range 500–1341 K, though Yarwood's rate constant is lower by as much as 30%. However, we are unable to judge whether this result is valid for $M = N_2 \text{O}$, NO, N_2 . This supports our extrapolation of Baulch's data, although it unfortunately does not help our estimation of the third-body efficiencies.

Reaction (R6) has a small effect on N_2O decomposition, and we include it only for completeness. Baulch et al. recommend a value only for 300–550 K, since information at higher temperatures is sparse. We have used this value at high temperature and have expanded the error limits by a factor of 2.

Reaction (R7) represents the diffusion of atomic oxygen to the walls of the furnace. It was concluded by Johnston that this is the dominant mechanism for O reaction at low temperature and pressure [36]. This conclusion is supported by data from Kaufman et al., which showed a decrease in NO production with decreasing pressure [38]. However, it is also evident from Kaufman's 1031 K data

set that this mechanism is important only for pressures below 30 Torr. At the temperatures and pressures which concern us (760 Torr, 1100–1500 K), the contribution of (R7) is negligible, and it is omitted from our model.

Reaction (R8) is the only reaction for which reliable data exist. The rate constant given by Baulch et al., which is taken from Rosser and Wise [35], is for the temperature range 600-2000 K. At silicon oxidation temperatures, this reaction reduces virtually all NO₂ generated by (R5) to NO and O₂.

To summarize, adequate information exists for (R6), (R7), and (R8). Information on (R1) has a gap in our region, but with the interpolation a reasonably accurate estimate is possible. The available data for (R2) are deficient with respect to collision-partner efficiencies, although we find that this reaction makes only a minor contribution to the decomposition process. Data for (R3) and (R4) are adequate, since the ratio k_3/k_4 is adequately defined, even if the error on absolute rates is large. Information on (R5) poses the greatest difficulty, since this is one of the most important decomposition reactions. As we show later, our experiments indicate that the recommended rate constant k_5 is somewhat low, but our results are still within its estimated error limits.

• N₂O half-life

The half-life of N_2O , combined with the gas-residence time at high temperature, determines whether the growth ambient at the Si surface contains atomic oxygen. Since atomic oxygen can remove previously incorporated nitrogen [29], this is an important factor in determining the final nitrogen profile of the oxynitride gate dielectric. Decomposition of N_2O at 900°C occurs on a time scale of seconds. The net result, from an examination of (R1–R8), is a mixture of N_2 , O_2 , and NO, with an NO_2 concentration of less than 50 ppm. Atomic oxygen is present only as an intermediate species in the decomposition of N_2O . Once the gases have reached steady state, no atomic oxygen is present.

The half-life of N_2O can be calculated from the rate of reaction for (R1). The results are plotted in **Figure 1** for atmospheric pressure. The darker regions indicate recommended values from Baulch et al. and their error limits [32], and the light central region from 1050 to 1300 K indicates our interpolation k_1^n between these two recommended values. The actual half-life most likely resides within the shaded band. We should note, however, that the observed N_2O half-life at the start of the decomposition of a volume of N_2O will be lower by a factor of 2, since each atomic oxygen generated by (R1) will consume an additional molecule of N_2O through (R3) and (R4). As decomposition progresses, the half-life will tend toward the value calculated from the rate constant.

• Isothermal NO production

In addition to the N₂O half-life, another critical parameter is the quantity of NO that is produced, since this determines the nitrogen density in the oxynitride. It has been known since the work of Briner et al. that the concentration of NO depends on the temperature at which decomposition occurs [39]. This can be viewed as competition between (R3), the only source of NO_x species, and (R2, R4–R7). As the temperature increases, (R3) and (R2) become comparatively more favorable reaction paths for atomic oxygen. This is evident from their higher activation energies (see Table 1).

We can quantify the amount of NO produced, as a function of isothermal decomposition temperature, through a numerical solution of the system of differential equations defined by the rate equations for (R1-R8), with the rate coefficients from Table 1. We have done this for isothermal decomposition, when the initial state is pure N₂O at one atmosphere and the pressure is kept constant. The resultant steady-state NO concentration, in terms of molar percentage, is shown in Figure 2 as a function of decomposition temperature. The squares were calculated from the base values for k_5 given in Table 1. The circles are calculated with k_5 at its upper limit, which we recommend in a subsequent section as a more accurate value. The vertical bars represent the maximal and minimal values from propagating the given error limits. The simulation indicates that little NO is produced below 800°C, and that beyond 1100°C the NO concentration seems to saturate near 30%. This limit results from competition between (R3) and (R4). The relative probability of either reaction path for atomic oxygen is near unity, so at most half of the oxygen in the system will form NO. This gives a maximum theoretical yield of 33% NO, with an NO/O, ratio of 2.

• Exothermic decomposition

The last critical parameter is the heat generated by $\rm N_2O$ decomposition. We have shown previously that this can have an important role in determining the decomposition temperature in a typical furnace [26]. This is because at sufficiently high flow rates the gas can self-heat by more than 200°C, which can substantially enhance NO production, thereby increasing the amount of N incorporated during oxynitridation. This exothermic phenomenon can be quantified and modeled, and we combine it with our reaction model in a later section. Two quantities are required for the thermal aspect of the model: the change in enthalpy ΔH^0 for (R1–R8), and the heat capacity at constant pressure $C_{\rm p}$. Both are weak functions of temperature. $C_{\rm p}$ can be approximated by the equation [40]

$$C_{\rm p} = a + bT + cT^2 + dT^{-2}$$
 [J/gK], (3)

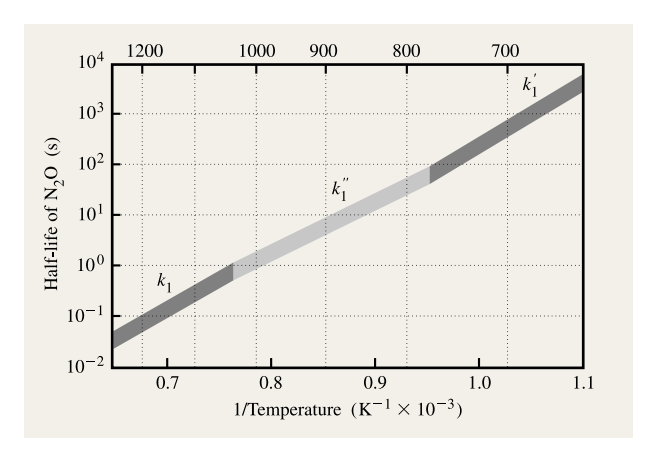


Figure 1

Half-life of N_2O at atmospheric pressure. Line widths represent error limits. The dark regions are calculated from k_1 and k_1' in Table 1 and Equation (2). The light central region, for which there are no direct reliable data, corresponds to k_1'' , interpolated from k_1 and k_1' . Owing to action by (R3) and (R4), the observed half-life in the early stages of decomposition will be as much as a factor of 2 lower, increasing monotonically with time.

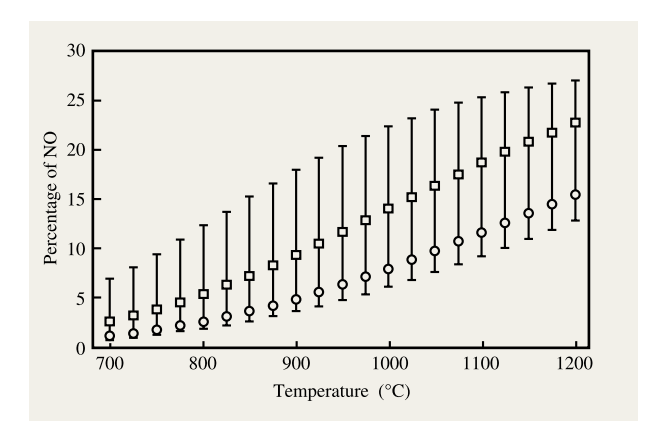


Figure 2

Percentage of NO as a function of isothermal decomposition temperature. Squares are calculated with the values from Table 1. Vertical bars represent the error limits given in the table. Circles represent our best-fit calculation using k_5^* , the upper error limit to k_5 . The trend clearly indicates increasing NO concentration with temperature, with the most rapid increase between 800°C and 1100°C, and saturation near 30% NO.

where T is the gas temperature and a, b, c, and d are coefficients given in **Table 2**. The enthalpy change ΔH^0 , which also has a weak temperature dependence, is described by the first-order approximation

Table 2 Heat capacity coefficients of the four relevant gases, in J/gK as defined by Equation (3). The coefficients for NO were calculated from raw data in [40]. NO₂ and O have been omitted, as their low relative concentrations have a negligible impact on the total heat capacity.

Gas	а	$b \times 10^{-3}$	$c \times 10^{-6}$	$d \times 10^5$	Source
N_2O	10.92	2.06	0	-2.04	[47]
N_2	6.76	0.606	0.13	0	[47]
O_2	8.27	0.258	0	-1.877	[47]
NO	30.1	3.91	0	0	[40]

Table 3 Coefficients for ΔH^0 , in J/mol, for the seven relevant reactions. The coefficients are defined in Equation (4). Calculated from data at 1000 and 1500 K, from Baulch et al. [32].

Reaction	$\alpha \times 10^{-5}$	β
(R1)	1.69	0
(R2)	-5.00	-5.94
(R3)	-1.47	-7.78
(R4)	-3.28	-8.06
(R5)	-3.09	-1.94
(R6)	-1.90	-4.00
(R8)	1.19	2.06

$$\Delta H^0 = \alpha + \beta T \qquad [J/mol]. \tag{4}$$

Here T is the gas temperature, and the coefficients α and β are given in **Table 3**. For adiabatic decomposition, at constant pressure, and with a starting N_2O temperature of $1000^{\circ}C$, the decomposition gases are heated by approximately $800^{\circ}C$, with only a weak dependence on initial temperature. On the scale of Figure 2, this is a significant change in temperature insofar as the final NO concentration is concerned. We therefore expect that the exothermic nature of decomposition has an important role in determining the final NO concentration.

Furnace processing

To model a standard horizontal tube furnace, we need detailed information on its temperature profile. These systems have a hot zone, kept at a uniform temperature, and an inlet, which may or may not have a controlled temperature profile. N_2O is fed into the inlet at a particular flow rate and is gradually heated to the temperature of the hot zone. When gas reaches the hot zone, generally after complete decomposition, it contacts and reacts with the wafer.

For O_2 and N_2 processing, as well as with any other stable gas, the temperature profile and shape of the inlet is inconsequential so long as the gas is sufficiently heated when it contacts the wafers. However, for N_2O processing,

the characteristics of the inlet affect the composition of the growth ambient. This is because, as we have shown, higher decomposition temperatures result in higher NO concentrations in the final decomposition product.

As the flow rate in a furnace is decreased, the heat-up time of the gas increases. We can therefore expect that, at low flow rates, the gas on average decomposes at a lower temperature, and NO generation is suppressed. At higher flow rates, we can expect an increase in the rate of heat generation due to the exothermic decomposition. This can heat gas at the inlet beyond the temperature of the furnace wall. Since higher temperatures increase the decomposition rate, this positive feedback can lead to autocombustion, in which all remaining N_2O is rapidly consumed. We have reported previously on these effects [26].

This behavior was confirmed by measuring the temperature profile and final NO concentration obtained by flowing N₂O through a 1-in. (ID) quartz tube, mounted in a resistively heated tube furnace. To measure the concentration of NO in the exhaust gas, we developed a titration loosely based on one given by Musgrave and Hinshelwood [41]. An evacuated flask is used to draw a controlled volume of furnace exhaust gas. A small amount of H₂O is introduced into the flask and allowed to stand for 30 minutes. Any NO in the gas combines with O, through the reverse of (R8), which dominates at room temperature, to form NO2. The NO2 undergoes an oxidation-reduction reaction with the water, forming one mole of HNO₃ for each mole of NO₂ [34, p. 354]. The amount of HNO₂ is determined through a volumetric acid-base titration. Knowing the amount of NO, and the volume of exhaust gas extracted, calculation of the NO concentration in the furnace is straightforward. Unfortunately, we were unable to calibrate this technique with either NO/NO, standards or an alternate measurement technique.

The gas-temperature profile in the furnace is measured in a separate experiment at various points along the central axis by placing a thermocouple in the gas stream. The gas-temperature profile is compared for $\rm N_2$ and $\rm N_2O$ in Figure 3. The distance is measured from the beginning of the heated region of the furnace. We used two nominal (set-point) furnace temperatures, 900°C and 1000°C. The observed gas temperatures in the front edge of the hot zone differed slightly from the set point, at 880°C and 1005°C respectively.

Since N_2 is stable at these temperatures, we can assume that the difference between the N_2 and N_2O curves represents the contribution of heat generated by decomposition. At 900°C, for a flow velocity of 0.65 cm/s¹

 $^{^1}$ We have based all quoted flow velocities on $\rm N_2O$ at room temperature and pressure (23°C, 1 atmosphere). The reader should recognize that the actual flow velocity of course increases with gas temperature, and as more gaseous species are created during decomposition.

this difference is at most 10°C, and indicates only mild heating over a broad region. Exothermic behavior at a similar level (a few °C) has been indirectly observed before in N₂O systems [42].

At a nominal furnace temperature of 1000°C , we measured gas-temperature profiles at two flow rates, 1.5 and 3.0 cm/s. The N_2 curves for the flow rates are similar. The $N_2\text{O}$ curve indicates that the exothermic decomposition heats the gas by slightly more than 200°C . The location of this hot region is approximately 5 cm into the tube at 1.5 cm/s, and 10 cm into the tube at 3.0 cm/s. This indicates similar residence times before the onset of self-heating for both flow velocities. In both hot regions, we also directly observed a white flame, attributable to the chemiluminescence of (R5) [38]. From the temperature profile, we conclude that for these conditions, much of the $N_2\text{O}$ decomposed at temperatures higher than 1100°C .

The fraction of NO at the end of decomposition was also measured for both nominal furnace temperatures, as a function of flow velocity. The results are shown in **Figure 4**. At a nominal temperature of 1000° C, the NO concentration varies from 4% to 19%, indicating an NO/O₂ ratio of 0.13 to 0.80, respectively. Such a large change in the growth ambient should have a dramatic effect on oxynitride growth. At 900° C, where the exothermic heating is less pronounced, the change in NO with flow rate is therefore smaller, from 2.2% to 4.4%. In both cases, the fraction of NO created saturates at a sufficiently high flow rate.

• Furnace modeling

To create a model for furnace N_2O decomposition, the thermodynamic information from Tables 2 and 3 can be combined with the reaction-rate data from Table 1. The principal difficulty is with quantifying heat exchange between the gas and the walls of the furnace. One method, employed by Hartig and Tobin [31], assumed a perfectly abrupt lateral transition in the wall of the furnace from 23°C to 950°C, with a heat-transfer rate proportional to $T_{\rm gas}-T_{\rm wall}$. We introduce a new method, based on the gas-temperature profiles obtained with flowing N_2 , as given in Figure 3.

The temperature profiles for N_2 at 1000° C, shown in Figure 3, are similar for both flow rates. We can therefore expect the N_2 profiles to be applicable over a wide range of flow velocities. For the N_2 gas, the temperature of the gas under steady flow is described by

$$\left. \frac{dT_{N_2}}{dx} \right|_{x=x'} = -h[T_{N_2}(x') - T_{w}(x')] \frac{1}{v(x')}.$$
 (5)

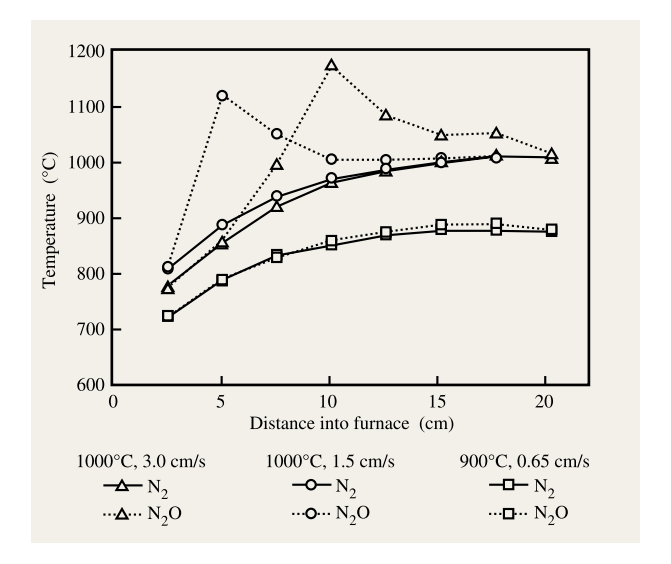


Figure 3

Gas-temperature profile of the 1-in. furnace under various conditions, as measured by a thermocouple in the gas stream. The difference between the N_2 and N_2O curves represents the contribution of heat generated by the exothermic decomposition of N_2O .

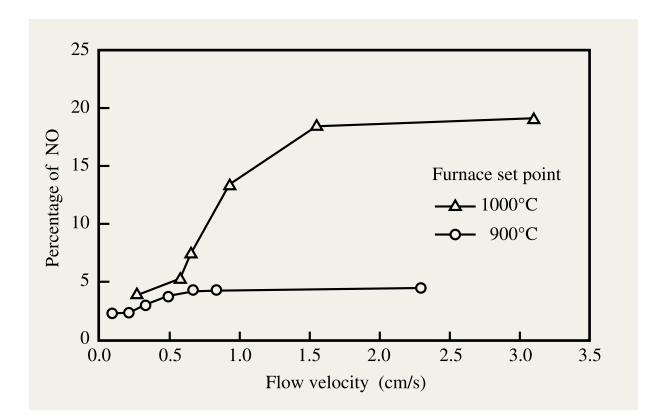


Figure 4

NO concentration as a function of flow velocity for the 1-in. tube furnace. Two nominal furnace temperatures are shown (1000°C and 900°C). The sharp rise in NO for the 1000°C curve is linked to the self-heating shown in Figure 3 for the same furnace.

Here $T_{\rm N_2}$ is a function of x, the distance into the furnace; x' is the point at which heat transfer is being evaluated; $T_{\rm w}$ is the temperature of the wall as a function of x; h is a parameter, in units of s⁻¹, characterizing the heat-transfer rate between the gas and the furnace; and v(x') is the flow velocity at x', given by

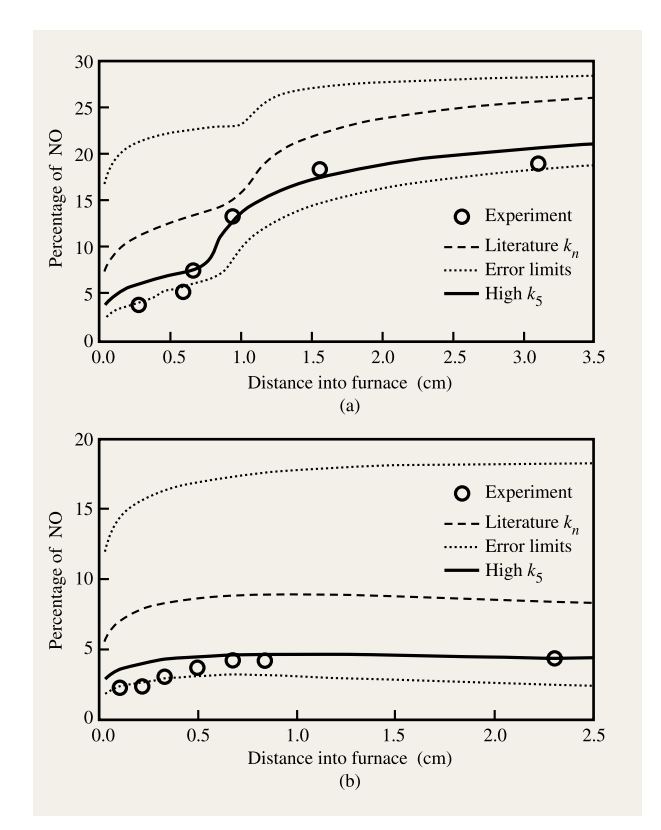


Figure 5

Model calculations (lines) vs. experimental results (circles) of NO concentration after completion of the decomposition, for nominal furnace temperatures of (a) 1000°C and (b) 900°C. Heat transfer is based on Equation (10) and the N₂ gas-temperature profiles in Figure 3. The best fit was with k_5^* , from Table 4. Results without adjustment (using literature values for k_n) and for upper and lower absolute error limits are also plotted. The slight drop-off in (b) at high flow velocities is due to incomplete decomposition of N₂O.

$$v(x') = \frac{dx}{dt} \bigg|_{x=x'}.$$
 (6)

The flow velocity v(x') depends on the flow rate at room temperature, the temperature of the gas at x', and the volume expansion due to the net creation of gaseous species during decomposition.

For N₂O, the temperature of the gas is described by

$$\left. \frac{dT_{N_2O}}{dx} \right|_{x=x'} = -\Gamma(x') - h[T_{N_2O}(x') - T_{w}(x')] \frac{1}{v(x')}, \tag{7}$$

where $\Gamma(x')$ is the temperature change due to the decomposition reactions:

$$\Gamma(x') \equiv \left[\sum_{i}^{(R_i)} \Delta H_i^0 r_i(x') \right] \left[\sum_{j} C_{p,j} n_j(x') \right]^{-1}.$$
 (8)

Here i is summed over all reactions, ΔH_i^0 is taken from Table 3, and r_i is the rate of reaction i. The summation in j is over the four abundant gaseous species $j = [N_2O, N_2, O_2, NO]$, with $C_{p,j}$ the heat capacity from Table 2, and n_j is the molar concentration of the jth species. The contributions of O and NO_2 are negligible, as their concentrations are in all cases less than 50 ppm, so we omit them from the calculation of the total C_p .

The effective temperature of the wall as a function of distance from the inlet can be solved from Equation (5):

$$T_{w} = \frac{dT_{N_2}}{dx} \bigg|_{y=y'} \frac{v(x')}{h} + T_{N_2}(x'). \tag{9}$$

Substituting this into Equation (7),

$$\frac{dT_{N_2O}}{dx}\bigg|_{x=x'} =
\left\{ -\Gamma(x') - h[T_{N_2O}(x') - T_{N_2}(x')] \right\} \frac{1}{v(x')} + \frac{dT_{N_2}}{dx} \quad . \quad (10)$$

With this equation, the temperature profile under pure N_2 flow, $T_{N_2}(x')$, can be combined with $\Gamma(x')$ to calculate $T_{N_2O}(x')$. This can yield more accurate results for the temperature profile of the gas than relying on approximate forms of $T_{m}(x')$.

With this treatment of the gas thermodynamics, and the reaction-rate coefficients discussed earlier, we can construct an accurate model for the decomposition of N₂O. Implementation of such a model is straightforward, and consists of coding the system of differential equations in a C⁺⁺ environment and applying appropriate boundary conditions. The principal difficulty is in dealing with the atomic oxygen, since it reacts on a much shorter time scale than N₂O decomposition, making direct numerical solution inefficient in this case. To overcome this difficulty, we calculate the generation rate of O and partition it between Reactions (R2-R6), based on evaluations of k_2 - k_6 . For (R2), which is second order in [O], we assume quasi-static conditions and estimate [O] based on total first- and second-order rate constants, solving the resulting quadratic equation. Evaluation of time-slice size effects and convergence indicates that our numerical method yields the correct solution.

Using the $\rm N_2$ temperature profiles from Figure 3, we calculated the final NO concentration as a function of flow rate. At 1000°C, the 1.5-cm/s and 3.0-cm/s $\rm N_2$ curves gave the same result to within 2%, so we used the 1.5-cm/s data set for all 1000°C NO calculations. The results are shown

in Figure 5(a). We found that the unaltered values from Table 1, given by the dashed line, were unable to explain our observations. However, we found that by using the upper error limit value for k_5 , denoted by k_5^* , agreement with our experimental results was excellent [dark solid line in Figure 5(a)]. The absolute error limits are given by the dotted lines.

Similar curves are given for 900°C in **Figure 5(b)**. Again, the unaltered rate constants from Table 1 cannot explain our observations, but by using the same upper error limit k_5^* we achieve good agreement. Note that the slight drop-off in the simulation results at higher flow rates is due to the incomplete decomposition of N_2O . The total length of the hot section in our experiment was only 40 cm, and at sufficiently high flow rates this did not provide a sufficient residence time to decompose all of the N_3O .

The model was also used to calculate the gas temperature as a function of distance into the furnace. At 1000°C, we used both N, temperature profiles to calculate corresponding N₂O gas temperatures at flow velocities of 1.5 cm/s and 3.0 cm/s. The total length of the furnace hot region, both simulated and real, is 40 cm. For the simulation, the value at the last data point is extended to this distance. We assume that no decomposition takes place until the first data point, at x = 2.54 cm. After this, the gas decomposes according to the reaction model, and the gas temperature is calculated as a function of distance into the furnace according to Equation (10). The results for 1000°C are shown in Figures 6(a) and 6(b), and in Figure 6(c) for 900°C and 0.65 cm/s. At 1000°C, hot regions similar to those observed experimentally are seen. However, both the magnitude of the temperature change and the location of the hot region disagree somewhat with our observations. We were unable to find model parameters which accurately reproduced our N₂O temperature profiles. This could perhaps be due to thermal conductivity of the temperature probe itself, which would limit its spatial resolution, thereby reducing the maximum observed temperature. Turbulence would have a similar effect. It could also be due to neglect of radial temperature gradients. On the other hand, at 900°C, agreement between our modeled gas-temperature results and our measurements is excellent.

To summarize the model calculations, we find that the recommended values from Table 1 are inadequate for modeling our system. The principal difficulty appears to be with k_5 , for which no direct rate information is available above 500 K. We therefore suggest that our extrapolation of published values is inaccurate, and we recommend use of the adjusted value k_5^* , given in **Table 4**, for modeling N_2O furnace processing. With this change, agreement between the simulation and our experimental observations is excellent for the dependence on flow rate of the NO concentration in fully decomposed N_2O . As for modeling

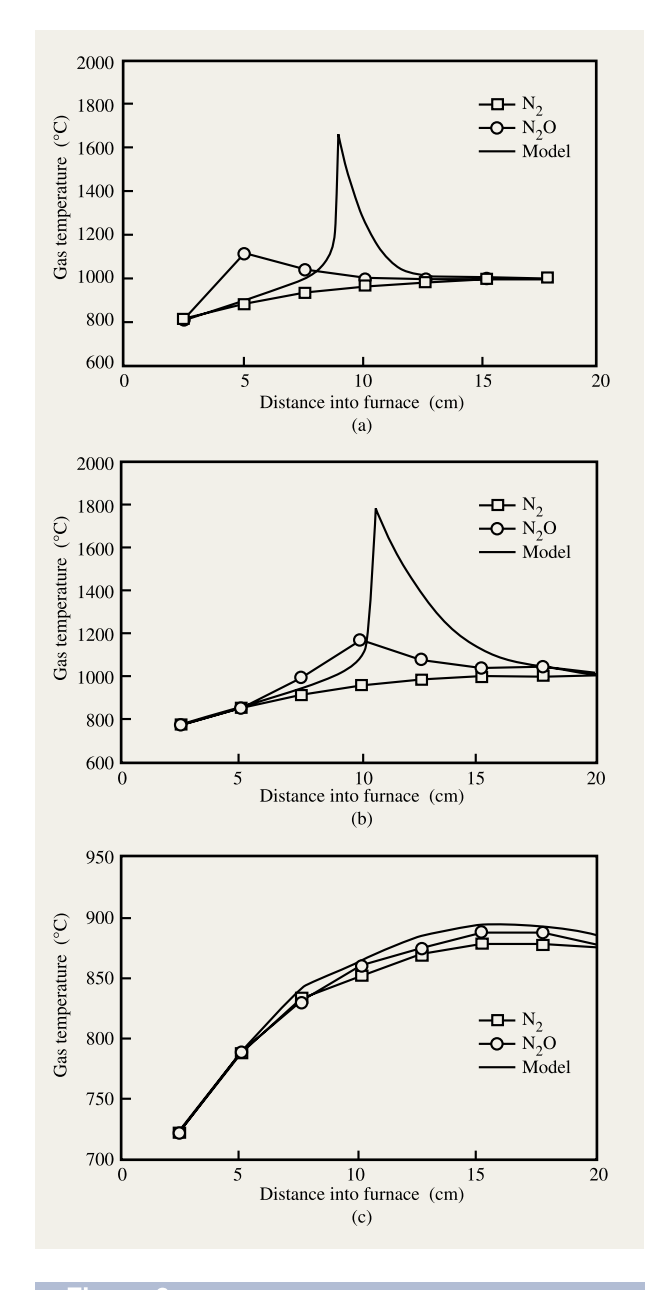


Figure 6

Calculated N₂O gas-temperature profile at (a) 1000°C, 1.5 cm/s; (b) 1000°C, 3.0 cm/s; and (c) 900°C, 0.65 cm/s for the same conditions as in Figure 3. The model correctly predicts the presence of a hot region for (a) and (b), but the location and magnitude disagree with measured values, perhaps owing to the neglect of turbulence and radial temperature gradients in our model.

the furnace gas temperature, we find that the model accurately predicts the general behavior of the system, namely the existence of a well-defined hot region in our 1000°C data set, and the absence of this effect in our measurement at 900°C. The precise location and

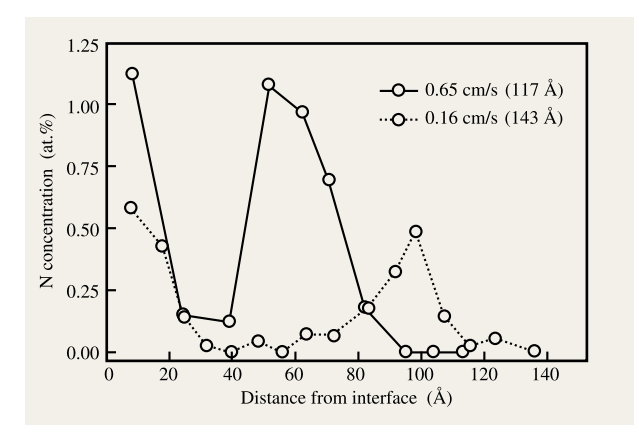


Figure 7

Nitrogen depth profile, measured using XPS, at two different flow velocities, 0.15 and 0.6 cm/s, in a standard MOS gate oxidation furnace. Growth was in $\rm O_2$ (5 min), $\rm N_2O$ (30 min), $\rm O_2$ (30 min), and $\rm N_2O$ (30 min), at 900°C. Total thicknesses are indicated. The increase in N content with flow rate is attributed to a higher NO/O₂ ratio in the growth ambient, as shown in Figure 6.

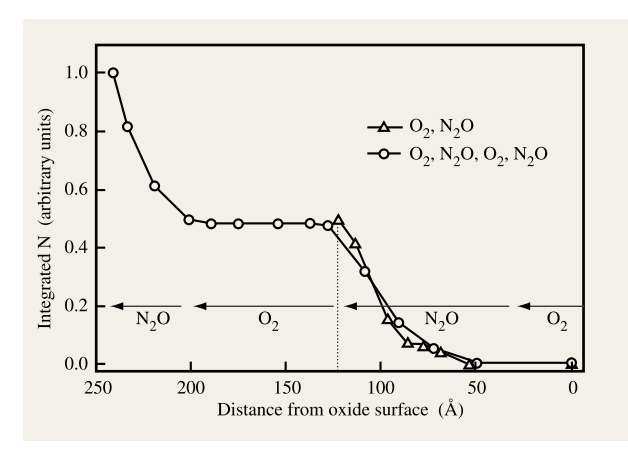


Figure 8

Integrated XPS N profiles for two N_2O furnace oxynitrides, on Si(111), one grown at 900°C in O_2 (5 min) and N_2O (30 min), and the other with additional steps in O_2 (30 min) and finally N_2O (30 min). The N concentration is integrated from the surface (right) toward the substrate (left). Arrow locations are approximate and indicate the growth ambient. No loss of N is observed, indicating stability in O_2 , N_2 , and NO, although the near-surface peak is seen to widen by several Å during subsequent processing.

magnitude of the hot region differ somewhat from our observations, probably owing to insufficient detail in our heat-transfer model, such as the neglect of radial thermal gradients in the furnace tube.

Table 4 Our recommended rate constant k_5^* for (R5), based on a comparison of model results with experimental observations. These represent the upper limits of error for k_5 from Table 1. Other rate constants did not require adjustment.

Rate constant	A (cm-mol-s)	$\frac{E_{\rm a}}{({ m eV})}$	Note
k_5^*	3.0×10^{15}	-0.081	$M = O_2$
	1.0×10^{16}	-0.081	$M = N_2$
	1.5×10^{16}	-0.081	$M = N_2O$, NO

Growth results

Our modeling results demonstrate that the NO concentration (and therefore the NO/O₂ ratio) depends strongly on the flow rate. Increasing the flow rate should therefore affect oxynitride growth in two ways. First, as the NO/O₂ ratio increases, more nitrogen should be incorporated into the film. Second, the growth rate of the film should decrease, owing to the higher concentrations of nitrogen. This results from the well-established fact that the rate of subsequent oxidation of oxynitrides is substantially lower than for pure oxides, with the retardation increasing with nitrogen content [43].

To confirm these effects, we grew a series of oxynitrides in a standard horizontal diffusion furnace used for MOS gate oxidation at the Cornell Nanofabrication Facility. All of the oxides were on Si(100) prime-grade wafers unless otherwise noted. The growth recipe follows one employed by Saks et al. [28], consisting of a 5-min O, step, 30-min N₂O, 30-min O₂, and finally 30-min N₂O, all at 900°C. The purpose for using this particular recipe was to obtain a bimodal nitrogen distribution in which the nitrogen incorporation or removal in either N₂O step can be monitored. In Figure 7, we show results for two flow rates, 1 and 4 SLM (standard liters per minute), corresponding to flow velocities of 0.15 and 0.6 cm/s. The N depth profile was measured with an XPS (X-ray photoelectron spectroscopy) HF spin-etch technique described elsewhere [9]. The total nitrogen content of the 0.6-cm/s oxynitride is approximately twice that of the 0.15-cm/s oxynitride. This increase in N content is attributed to the higher NO/O, ratio in the growth ambient at the higher flow rate.

The effect of flow rate can also be seen in the total thicknesses of the oxynitrides in Figure 7. For this study, an additional film was grown at 0.3 cm/s (2 SLM). Ellipsometric thicknesses for the 0.15-, 0.3-, and 0.6-cm/s films were 143 Å, 139 Å, and 117 Å, respectively. We attribute this change in growth rate to the mechanism suggested by Green et al. [43], in which incorporated N either blocks access to interfacial reaction sites or blocks transport of oxidant species to the interface, thereby reducing the growth rate.

The presence of the second near-surface nitrogen peak in Figure 7 also demonstrates the stability of previously incorporated nitrogen during high-temperature exposure to NO, O₂, and N₂. We have investigated this stability more directly, on Si(111), using a similar growth recipe. Two wafers were exposed at 900°C to O₂ (5 min), then N_2O (30 min). One of the wafers was profiled with XPS. The other was exposed again at 900°C to O₂ (5 min) and finally N₂O (30 min), and also profiled with XPS. The integrated N concentration for both wafers is shown in Figure 8. Within the accuracy of our profiling technique (10%), there is no evidence for N loss, and N appears to be stable in both O₂ and completely dissociated N₂O. We note, however, that the near-surface nitrogen peak widens by several Å during subsequent processing. A similar widening was reported by Ganem et al. [30], who attributed it to defect-mediated slow diffusion.

The variation in N content with flow rate shown in Figure 7 can be a useful tool for controlling oxynitride properties. According to our NO measurements, the ${\rm NO/O_2}$ ratio can be controlled by at least a factor of 6 in a properly designed furnace. This ratio directly affects the amount of nitrogen incorporated during oxynitride growth, and although this may not translate directly into a factor of 6 change in nitrogen content, it demonstrates that flow rate can be as important as temperature in determining nitrogen content, as shown in Figure 7.

The variation with temperature of N content is a separate issue. There is some evidence that, in pure NO, the ratio of nitrogen to oxygen incorporated into an oxynitride increases with temperature [44]. This might seem to explain why higher-temperature N_2O processing produces higher nitrogen concentrations. However, oxynitride N content shows a much stronger dependence on temperature with N_2O than it does with NO [20, 24]. In particular, at or just below $1000^{\circ}C$ there is a rapid increase in N content, seen both in Figure 2 and in the work by Matsumura and Nishioka [24]. This suggests that the N content is affected by temperature dependencies both in the NO/O_2 ratio and in the kinetics of NO and O_2 reactions at the Si/SiO₂ interface.

Rapid thermal and high-flow-rate processing

Rapid thermal processing is an alternative technique commonly used to grow oxynitrides with N_2O . Films grown in this manner differ markedly from furnace oxynitrides in two respects: 1) nitrogen is incorporated only within 20-30 Å of the substrate interface, compared to broader distributions in furnace oxynitrides [23, 29, 45]; 2) the nitrogen is incorporated at higher densities at a given growth temperature [29]. Compared to the furnace, the RTP therefore concentrates more nitrogen where it is most beneficial for the enhancement of electrical reliability: at the Si/SiO₂ interface [9, 45].

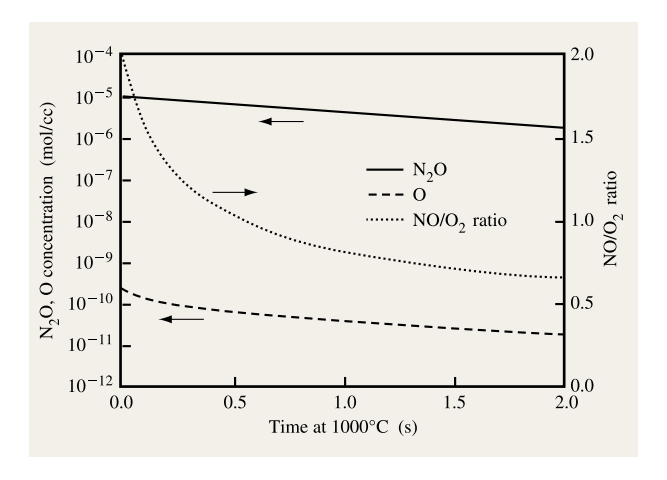


Figure 9

Gas species, as a function of time in decomposing N_2O , for isothermal decomposition at 1000°C. The early stages should be similar to an RTP growth ambient. The N_2O and O concentrations are plotted on the left axis, NO/O_2 ratio on the right. At all temperatures, the initial NO/O_2 ratio is exactly 2.

The key to understanding the first effect is again the decomposition chemistry. In an RTP, there is a constant influx of fresh N2O to the wafer surface, and the residence time for this gas is short. The gas near the wafer, furthermore, should be at or near the temperature of the wafer because of its low mass density compared to solid silicon. We can therefore expect that this gas resembles the early stages of our isothermal decomposition model. Using this model, we have calculated the concentration of N₂O and O, and the NO/O, ratio, as a function of time. The results, shown in Figure 9 for a wafer temperature of 1000°C, indicate that at the start of decomposition the NO/O, ratio is universally 2, decreasing monotonically with time. This much is evident from an examination of the available reaction pathways for O. At the onset of decomposition, half of the O will react by (R3), and half by (R4), giving an NO/O, ratio of 2. Atomic oxygen, at this temperature, is initially present at 20 ppma considerable concentration considering the highly reactive nature of this species.

The higher density of N in RTP-grown oxynitrides, as compared to furnace oxynitrides, results from this enhanced NO/O_2 ratio; in an RTP process, the time between the onset of N_2O decomposition and contact with the wafer surface is short compared to the half-life of N_2O . This translates directly to a higher density of N incorporated into the film. How far decomposition progresses in an RTP, and whether N_2O interacts directly with the wafer, are not yet known, and therefore a more

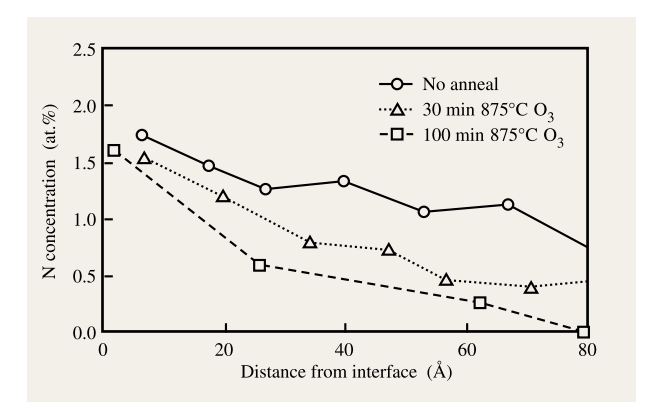


Figure 10

XPS N profiles, showing the effect of atomic oxygen exposure on previously incorporated nitrogen. Initial sample is a 130-Å furnace-grown N_2O oxynitride. Two samples were exposed to a 0.9-Torr mixture of 10% $O_3/90\%$ O_2 at 875°C, for 30 and 100 min. The N profile indicates a gradual loss of N due to atomic oxygen from ozone decomposition. The same mechanism, involving O from (R1), causes N loss during N_2O RTP.

complete model of RTP systems is not feasible at this point.

The other distinguishing feature of RTP oxynitrides is the localization of N to within 20--30~Å of the substrate interface. As additional oxynitride is grown, this N peak is translated deeper into the wafer. Some process is therefore removing nitrogen after it has been incorporated. However, as we demonstrated in Figure 8, N incorporation is stable in O_2 , N_2 , and NO. We conclude that there is a chemical reaction which is specific to the RTP. The only species which are present at the wafer during RTP, and absent from the wafer in the furnace, are atomic oxygen from Reaction (R1) and N_2O .

To test the possibility that atomic oxygen might be responsible for N loss, we exposed a series of oxynitrides to ozone at high temperature [29]. The samples were mounted in a vacuum system with a base pressure of 10^{-7} Torr, and heated from the back side to 875°C. The annealing ambient was a mixture of 10% O₃/90% O₂, at a pressure of 0.9 Torr. At this temperature, ozone decomposes rapidly into O₂ and O. Two samples were annealed for 30 min and 100 min and the resulting XPS N profiles are compared with that for the as-grown N₂O furnace oxynitride in **Figure 10**. The results indicate a gradual loss of N, with the fraction lost increasing toward the surface.

High-flow-rate furnaces, by which we mean furnaces where the gas-residence time is of the order of the half-life of N_2O , deserve some special mention. Owing to their short residence time, some N_2O survives to reach the

wafer, and therefore the growth ambient contains atomic oxygen. Oxynitrides grown in these systems are therefore indistinguishable from RTP oxynitrides, in that N is localized to the substrate interface due to removal of bulk N by atomic oxygen [29]. This caused some confusion in the case of Saks et al. [28], who erroneously attributed N removal to NO. Some of this confusion is from the N₂O half-life calculation of Tobin et al. [25]. By extrapolating data from Lewis and Hinshelwood [46], they estimated the half-life to be 2 s at 900°C. However, Lewis's values are effective half-lives at the start of decomposition (first few seconds). Our analysis demonstrates that this is not a simple exponential process, and we therefore suggest a somewhat longer half-life of 4–9.5 s, as calculated from k_1 , with an observed half-life in the early stages (first few seconds) of decomposition of 2-5 s. As discussed earlier, the effective half-life increases monotonically with time. Other arguments against removal of N by O which have been based on low absolute concentrations of O [28] do not appear to be appropriate. For a first-order reaction for the removal of incorporated nitrogen, with rate constant k, the relevant quantity is k[O], not [O]. In other words, O is a highly reactive species, and its low concentration is a reflection of its quick removal through reaction with other gaseous species or by reaction with the wafer.

Conclusion

The gas-phase model which we have presented accounts for the salient features of N_2O decomposition and oxynitride growth. We find that information on the relevant rate constants in Table 1 is sparse, particularly for (R5). First-principles modeling of this system is therefore unreliable. However, by comparing model calculations to experimental determinations of gas temperature and NO concentration as a function of flow rate and temperature, we are able to adjust the values in Table 1 within their estimated error limits and obtain good agreement. In particular, we recommend a somewhat higher value for k_5 , given as k_5^* in Table 4, than is extrapolated from low temperature.

One critical element of the model is quantifying heat transfer by referencing the $\rm N_2O$ gas temperature to the measured gas-temperature profile of a furnace flowing $\rm N_2$, via Equation (10). The necessity of this step is a reflection of the fact that most of the $\rm N_2O$ decomposes in or near the gas inlet. The precise temperature profile at the inlet is therefore of the utmost importance in determining the final NO content in the fully decomposed $\rm N_2O$ products. At high flow rates, the gas can self-heat by more than $200^{\circ}\rm C$, causing a rapid rise in NO. At low flow rates, the self-heating is minimal, and much of the gas decomposes at the cooler temperatures of the inlet.

The results of our N₂O thermal decomposition model confirm the basic observation that NO concentration increases with both flow rate and nominal furnace temperature. The other important factor is N₂O half-life and residence time at high temperature. The first step in decomposition involves the creation of atomic oxygen. This highly reactive species can remove previously incorporated nitrogen in the silicon oxynitride. This mechanism is responsible for the localization of nitrogen near the Si interface in rapid thermal and high-flow-rate furnace processing.

Acknowledgments

This research was supported by the Semiconductor Research Corporation. Additional support was provided by the National Science Foundation, through the use of the Cornell Nanofabrication Facility and the use of the facilities of the Cornell Materials Science Center.

References

- The National Technology Roadmap for Semiconductors, Semiconductor Industry Association, San Jose, CA, 1997.
- T. Hori, H. Iwasaki, and K. Tsuji, "Electrical and Physical Properties of Ultrathin Reoxidized Nitrided Oxides Prepared by Rapid Thermal Processing," *IEEE Trans. Electron Devices* 36, 340 (1989).
- 3. H. Hwang, W. Ting, B. Maiti, D.-L. Kwong, and J. Lee, "Electrical Characteristics of Ultrathin Oxynitride Gate Dielectric Prepared by Rapid Thermal Oxidation of Si in N₂O," *Appl. Phys. Lett.* **57**, 1010 (1990).
- Z. Liu, H.-J. Wann, P. K. Ko, C. Hu, and Y. C. Cheng, "Effects of N₂O Anneal and Reoxidation on Thermal Oxide Characteristics," *IEEE Electron Device Lett.* 13, 402 (1992)
- Z.-Q. Yao, H. B. Harrison, S. Dimitrijev, D. Sweatman, and Y. T. Yeow, "High Quality Ultrathin Dielectric Films Grown on Silicon in a Nitric Oxide Ambient," *Appl. Phys. Lett.* 64, 3584 (1994).
- Y. Okada, P. J. Tobin, K. G. Reid, R. I. Hedge, B. Maiti, and S. A. Ajuria, "Gate Oxynitride Grown in Nitric Oxide (NO)," *IEDM Tech. Digest*, p. 105 (1994).
- D. Bouvet, P. A. Clivaz, M. Dutoit, C. Coluzza, J. Almeida, G. Margaritondo, and F. Pio, "Influence of Nitrogen Profile on Electrical Characteristics of Furnace or Rapid Thermally Nitrided Silicon Dioxide Films," J. Appl. Phys. 79, 7114 (1996).
- H. Hwang, W. Ting, D.-L. Kwong, and J. Lee, "Improved Reliability Characteristics of Submicrometer nMOSFET's with Oxynitride Gate Dielectric Prepared by Rapid Thermal Oxidation in N₂O," *IEEE Electron Device Lett.* 12, 495 (1991).
- E. C. Carr and R. A. Buhrman, "Role of Interfacial Nitrogen in Improving Thin Silicon Oxides Grown in N₂O," Appl. Phys. Lett. 63, 54 (1993).
- Z.-J. Ma, Z. H. Liu, J. T. Krick, H. J. Huang, Y. C. Cheng, C. Hu, and P. K. Ko, "Optimization of Gate Oxide N₂O Anneal for CMOSFET's at Room and Cryogenic Temperatures," *IEEE Trans. Electron Devices* 41, 1364 (1994).
- M. Bhat, J. Kim, J. Yan, G. W. Yoon, K. Han, and D. L. Kwong, "MOS Characteristics of Ultrathin NO-Grown Oxynitrides," *IEEE Electron Device Lett.* 15, 421 (1994).
- 12. T. Matsuoka, S. Taguchi, H. Ohtsuka, K. Taniguchi, C. Hamaguchi, S. Kakimoto, and K. Uda, "Hot-Carrier-

- Induced Degradation of N₂O-Oxynitrided Gate Oxide NMOSFET's," *IEEE Trans. Electron Devices* **43**, 1364 (1996).
- E. Cartier, D. A. Buchanan, and G. J. Dunn, "Atomic Hydrogen-Induced Interface Degradation of Reoxidized-Nitrided Silicon Dioxide on Silicon," *Appl. Phys. Lett.* 64, 901 (1994).
- T. Aoyama, K. Suzuki, H. Tashiro, Y. Toda, T. Yamazaki, Y. Arimoto, and T. Ito, "Boron Diffusion Through Pure Silicon Oxide and Oxynitride Used for Metal-Oxide-Semiconductor Devices," *J. Electrochem. Soc.* 140, 3624 (1993).
- D. Mathiot, A. Straboni, E. Andre, and P. Debenest, "Boron Diffusion Through Thin Gate Oxides: Influence of Nitridation and Effect on the Si/SiO₂ Interface Electrical Characteristics," J. Appl. Phys. 73, 8215 (1993).
- T. Aoyama, K. Suzuki, H. Tashiro, Y. Toda, T. Yamazaki, K. Takasaki, and T. Ito, "Effect of Fluorine on Boron Diffusion in Thin Silicon Dioxides and Oxynitrides," J. Appl. Phys. 77, 417 (1995).
- S. Nedélec, D. Mathiot, M. Gauneau, and A. Straboni, "Boron Diffusion in SiO₂ Based Dielectric Thin Layers," J. Non-Cryst. Solids 187, 106 (1995).
- K. A. Ellis and R. A. Buhrman, "Monte Carlo Simulation of Boron Diffusion in Silicon Oxides and Oxynitrides," *Proc. Electrochem. Soc.* 10-97, 370 (1997).
- K. A. Ellis and R. A. Buhrman, "Boron Diffusion in Silicon Oxides and Oxynitrides," *J. Electrochem. Soc.* 145, 2068 (1998).
- G. Weidner and D. Krüger, "Temperature Variation of Nitrogen Content by N₂O-Rapid Thermal Processing of Silicon and of Silicon Oxide on Silicon," *Microelectron. J.* 24, 409 (1993).
- T. Y. Chu, W. T. Ting, J. Ahn, and D. L. Kwong, "Thickness and Compositional Nonuniformities of Ultrathin Oxides Grown by Rapid Thermal Oxidation of Silicon in N₂O," *J. Electrochem. Soc.* 138, L13 (1991).
- P. Lange, H. Bernt, E. Hartmannsgruber, and F. Naumann, "Growth Rate and Characterization of Silicon Oxide Films Grown in N₂O Atmosphere in a Rapid Thermal Processor," J. Electrochem. Soc. 141, 259 (1994).
- H. T. Tang, W. N. Lennard, M. Zinke-Allmang, I. V. Mitchell, L. C. Feldman, M. L. Green, and D. Brasen, "Nitrogen Content of Oxynitride Films on Si(100)," *Appl. Phys. Lett.* 64, 3473 (1994).
- M. Matsumura and Y. Nishioka, "Growth Kinetics of Ultra-Thin N₂O Oxynitrides for Gate Insulator," *Appl. Surf. Sci.* 117/118, 136 (1997).
- P. J. Tobin, Y. Okada, S. A. Ajuria, V. Lakhotia, W. A. Feil, and R. I. Hedge, "Furnace Formation of Silicon Oxynitride Thin Dielectrics in Nitrous Oxide (N₂O): The Role of Nitric Oxide (NO)," *J. Appl. Phys.* 75, 1811 (1994).
- K. A. Ellis and R. A. Buhrman, "Furnace Gas-Phase Chemistry of Silicon Oxynitridation in N₂O," *Appl. Phys. Lett.* 68, 1696 (1996).
- P. Lange, H. Boness, and M. Hendriks, "Oxynitridation of Silicon and Postnitridation of Thermal Silicon Oxide in N₂O in a Vertical Furnace," *J. Electrochem. Soc.* 144, 3650 (1997).
- N. S. Saks, D. I. Ma, and W. B. Fowler, "Nitrogen Depletion During Oxidation in N₂O," *Appl. Phys. Lett.* 67, 374 (1995).
- E. C. Carr, K. A. Ellis, and R. A. Buhrman, "N Depth Profiles in Thin SiO₂ Grown or Processed in N₂O: The Role of Atomic Oxygen," *Appl. Phys. Lett.* 66, 1492 (1995).
- J.-J. Ganem, S. Rigo, I. Trimaille, I. J. R. Baumvol, and F. C. Stedile, "Dry Oxidation Mechanisms of Thin Dielectric Films Formed Under N₂O Using Isotopic Tracing Methods," *Appl. Phys. Lett.* 68, 2366 (1996).

- 31. M. J. Hartig and P. J. Tobin, "A Model for the Gas-Phase Chemistry Occurring in a Furnace N₂O Oxynitride Process," *J. Electrochem. Soc.* **143**, 1753 (1996).
- 32. D. L. Baulch, D. D. Drysdale, D. G. Horne, and A. C. Lloyd, Eds., *Evaluated Kinetic Data for High Temperature Reactions*, Vol. 2, Buttersworths, London, 1973.
- 33. D. L. Baulch, D. D. Drysdale, J. Duxbury, and S. Grant, Eds., *Evaluated Kinetic Data for High Temperature Reactions*, Vol. 3, Buttersworths, London, 1976.
- K. Jones, Comprehensive Inorganic Chemistry, Pergamon, Oxford, 1973.
- 35. W. A. Rosser, Jr. and H. Wise, "Thermal Decomposition of Nitrogen Dioxide," *J. Chem. Phys.* **24**, 493 (1956).
- 36. H. S. Johnston, "Interpretation of the Data on the Thermal Decomposition of Nitrous Oxide," *J. Chem. Phys.* **19,** 663 (1951).
- 37. G. Yarwood, J. W. Sutherland, M. A. Wickramaaratchi, and R. B. Klemm, "Direct Rate Constant Measurement for the Reaction O + NO + Ar \rightarrow N₂O + Ar at 300–1341 K," *J. Phys. Chem.* **95**, 8771 (1991).
- 38. F. Kaufman, N. J. Gerri, and R. E. Bowman, "Role of Nitric Oxide in the Thermal Decomposition of Nitrous Oxide," *J. Chem. Phys.* **25**, 106 (1956).
- 39. E. Briner, Ch. Meiner, and A. Rothen, "Recherches sur la Decomposition Thermique du Protoxyde et de l'Oxyde d'Azote," *J. Chim. Phys.* **23**, 609 (1926).
- D. R. Lide and H. V. Kehiaian, Eds., CRC Handbook of Thermophysical and Thermochemical Data, CRC Press, Boca Raton, FL, 1994.
- 41. F. F. Musgrave and C. N. Hinshelwood, "The Thermal Decomposition of Nitrous Oxide, and Its Catalysis by Nitric Oxide," *Proc. Roy. Soc. A* **165**, 23 (1932).
- T. S. Chao, W. H. Chen, S. C. Sun, and H. Y. Chang, "An Exothermic Phenomenon of Silicon Oxidation by N₂O," *J. Electrochem. Soc.* 140, L160 (1993).
- M. L. Green, D. Brasen, L. C. Feldman, W. Lennard, and H.-T. Tang, "Effect of Incorporated Nitrogen on the Kinetics of Thin Rapid Thermal N₂O Oxides," *Appl. Phys. Lett.* 67, 1600 (1995).
- E. P. Gusev, H. C. Lu, T. Gustafsson, E. Garfunkel, M. L. Green, and D. Brasen, "The Composition of Ultrathin Silicon Oxynitrides Thermally Grown in Nitric Oxide," J. Appl. Phys. 82, 896 (1997).
- 45. Y. Okada, P. J. Tobin, V. Lakhotia, W. A. Feil, S. A. Ajuria, and R. I. Hedge, "Relationship Between Growth Conditions, Nitrogen Profile, and Charge to Breakdown of Gate Oxynitrides Grown from Pure N₂O," *Appl. Phys. Lett.* 63, 194 (1993).
- R. M. Lewis and C. N. Hinshelwood, "The Thermal Decomposition of Nitrous Oxide," *Proc. Roy. Soc. A* 168, 441 (1938).
- 47. R. C. Weast, Ed., CRC Handbook of Chemistry and Physics, 67 edition, CRC Press, Boca Raton, FL, 1986.

Received September 1, 1997; accepted for publication June 26, 1998

Kenneth A. Ellis Bell Laboratories, 600 Mountain Avenue, Murray Hill, New Jersey 07974 (KAEllis@lucent.com). Dr. Ellis received his B.S. degree in physics from the Massachusetts Institute of Technology in 1993. He received his Ph.D. degree in physics from Cornell in 1998. His early work was on the gas-phase chemistry of silicon oxynitridation, and his more recent work has been on understanding boron diffusion in silicon oxides and oxynitrides. Currently he is a postdoctoral member of the technical staff at Lucent Technologies' Bell Laboratories, working in the Applied Materials Research Department. His current research interests include thin-film ferromagnetism, diffusion in oxides, and the growth of MOSFET gate dielectrics.

Robert A. Buhrman School of Applied and Engineering Physics, Cornell University, Ithaca, New York 14853 (RAB8@cornell.edu). Dr. Buhrman received his undergraduate degree in engineering physics from Johns Hopkins University in 1967 and his Ph.D. degree in applied physics from Cornell University in 1973. Subsequently that year he joined the faculty of Applied and Engineering Physics at Cornell. He is currently the John Edson Sweet Professor of Engineering and Director of the School of Applied and Engineering Physics at Cornell. He is also Chair of the Executive Committee of the Cornell Nanofabrication Facility. Dr. Buhrman's current research interests include gate dielectric studies, superconducting thin films and devices, thin-film magnetism, and investigations of electrical transport in metallic and semiconductor nanostructures.